Hindawi
Journal of Sensors
Volume 2024, Article ID 9832826, 1 page
https://doi.org/10.1155/2024/9832826

Retraction

Retracted: Enhance-Net: An Approach to Boost the Performance of Deep Learning Model Based on Real-Time Medical Images

Journal of Sensors

Received 23 January 2024; Accepted 23 January 2024; Published 24 January 2024

This article has been retracted by Hindawi following an investigation undertaken by the publisher [1]. This investigation has uncovered evidence of one or more of the following indicators of systematic manipulation of the publication process:

(1) Discrepancies in scope
(2) Discrepancies in the description of the research reported
(3) Discrepancies between the availability of data and the research described
(4) Inappropriate citations
(5) Incoherent, meaningless and/or irrelevant content included in the article
(6) Manipulated or compromised peer review

The presence of these indicators undermines our confidence in the integrity of the article's content and we cannot, therefore, vouch for its reliability. Please note that this notice is intended solely to alert readers that the content of this article is unreliable. We have not investigated whether authors were aware of or involved in the systematic manipulation of the publication process.

Wiley and Hindawi regrets that the usual quality checks did not identify these issues before publication and have since put additional measures in place to safeguard research integrity.

We wish to credit our own Research Integrity and Research Publishing teams and anonymous and named external researchers and research integrity experts for contributing to this investigation.

The corresponding author, as the representative of all authors, has been given the opportunity to register their agreement or disagreement to this retraction. We have kept a record of any response received.

References

[1] V. Narayan, P. K. Mall, A. Alkhayyat, K. Abhishek, S. Kumar, and P. Pandey, "Enhance-Net: An Approach to Boost the Performance of Deep Learning Model Based on Real-Time Medical Images," *Journal of Sensors*, vol. 2023, Article ID 8276738, 15 pages, 2023.

Hindawi
Journal of Sensors
Volume 2023, Article ID 8276738, 15 pages
https://doi.org/10.1155/2023/8276738

Research Article

Enhance-Net: An Approach to Boost the Performance of Deep Learning Model Based on Real-Time Medical Images

Vipul Narayan,[1] **Pawan Kumar Mall**,[2] **Ahmed Alkhayyat**,[3] **Kumar Abhishek**,[4] **Sanjay Kumar**,[5] **and Prakash Pandey**[6]

[1]*Galgotias University, Greater Noida, India*
[2]*Lovely Professional University, India*
[3]*College of Technical Engineering, The Islamic University, Najaf, Iraq*
[4]*National Institute of Technology Patna, India*
[5]*Rajkiya Engineering College, Azamgarh, India*
[6]*Graduate School of Engineering, Mid-West University, Nepal*

Correspondence should be addressed to Prakash Pandey; prakash.pandey@mu.edu.np

Received 17 August 2022; Revised 28 September 2022; Accepted 12 October 2022; Published 2 May 2023

Academic Editor: Sweta Bhattacharya

Real-time medical image classification is a complex problem in the world. Using IoT technology in medical applications assures that the healthcare sectors improve the quality of treatment while lowering costs via automation and resource optimization. Deep learning is critical in categorizing medical images, which is accomplished by artificial intelligence. Deep learning algorithms allow radiologists and orthopaedic surgeons to make their life easier by providing them with quicker and more accurate findings in real time. Despite this, the classic deep learning technique has hit its performance limits. For these reasons, in this research, we examine alternative enhancement strategies to raise the performance of deep neural networks to provide an optimal solution known as Enhance-Net. It is possible to classify the experiment into six distinct stages. Champion-Net was chosen as a deep learning model from a pool of benchmark deep learning models (EfficientNet: B0, MobileNet, ResNet-18, and VGG-19). This stage helps choose the optimal model. In the second step, Champion-Net was tested with various resolutions. This stage helps conclude dataset resolution and improves Champion-Net performance. The next stage extracts green channel data. In the fourth step, Champion-Net combines with image enhancement algorithms CLAHE, HEF, and UM. This phase serves to improve Enhance-performance. The next stage compares the Enhance-Net findings to the lightness order error (LoE). In Enhance-Net models, the current study combines image enhancement and green channel with Champion-Net. In the final step, radiologists and orthopaedic surgeons use the trained model for real-time medical image prediction. The study effort uses the musculoskeletal radiograph-bone classification (MURA-BC) dataset. Classification accuracy of Enhance-Net was determined for the train and test datasets. These models obtained 98.02 percent, 94.79 percent, and 94.61 percent accuracy, respectively. The 96.74% accuracy was achieved during real-time testing with the unseen dataset.

1. Introduction

The IoT in medical imaging allows detection and remedial steps to be conducted in real time with the convenience of autoanalyzing imaging equipment characteristics. Numerous research has been conducted in medical imaging to investigate the use of various deep neural network- (DNN-) based models to categorize or diagnose illnesses. DNNs have been used to classify and diagnose diseases in the past. Deep neural networks have been successfully applied to the classification and diagnosis of illnesses in various types of medical conditions [1–6]. In recent years, image classification, segmentation, and detection techniques have been coupled with an era in which diagnostic medical imaging is becoming increasingly popular and essential for medical diagnosis [7, 8]. A fundamental challenge with medical imaging, on the other hand, is the availability of big datasets with trustworthy ground truth analysis, which is difficult to

come by. Deep learning models (DLMs) have aided in the development of a number of advancements in the field of image classification [9–13].

According to a recent study [14], the depth of a network-oriented model is crucial for critical datasets. This demonstrates that a network-based model's depth is crucial for challenging datasets. The debate about shallow vs. deep nets has raged in DLMs for a long time. The issue of decreased feature reuse arises while training extremely deep learning models [15–17]. This makes the training procedure for these models difficult. In [18], to obtain higher accuracy and minimal error in training loss, create a deep learning model with the ideal resolution, depth, and breadth combination. Several approaches have been proposed throughout the literature to deal with raindrop detection problems. However, most of these do not consider the following system requirements: high detection rate, real-time constraint, and robustness under dynamic environments.

A DLM technique called Enhance-Net is proposed to enhance the overall performance of musculoskeletal radiographs and X-ray pictures in a clinical setting. The most interesting aspect of this study is the evaluation of the influence of three distinct image enhancement algorithms (CLAHE, UM, and HEF) on green channel grayscale medical musculoskeletal radiography X-ray images for DLMs. The following sections of the paper are divided into seven phases: in Section 3, we discussed the materials and processes that were utilized to create the proposed model, which was interesting. In Section 4, we have gone into further detail about the suggested model. In Section 5, we went through the simulation, the results, and the validation process in great depth. In Section 6, we have discussed about real-time verification and result outcome. The final segment of Section 7 was dedicated to the conclusion and future work.

2. Related Work

In [19], the study tested the model's efficiency by extending the depth (16-20 layers) on ImageNet Challenge held in 2014 on different datasets. The deep learning model's error rate reaches saturation at the 19th layer. The authors created a residual learning model to make training deeper networks easier [20]. On the ImageNet test dataset, the model has a 3.57 percent error rate [20]. The model designer may create the optimal size model constraint in the design [5, 21–23]. In [18], the study offers a scaling technique that uses a compound coefficient to scale evenly using three key parameters (width, depth, and resolution) simultaneously.

When IoT technology is used in healthcare applications, it helps improve the quality of care and lower costs through automation and better use of resources. IoT in medical imaging makes it easy to find out what is wrong and take steps to fix it in real time. This is made possible by the auto-analysis of the imaging equipment's parameters [24]. The Internet of things (IoT) lets people develop systems that use sensors, connected devices, and the Internet. In the ICU, monitoring patients is an essential thing to do. Even a slight delay in making decisions about how to treat a patient could cause permanent disability or even death. Most ICU devices have sensors that can measure different health parameters, but it is still hard to keep an eye on them all the time. We are proposing a system based on the Internet of things (IoT), which can help speed up communication, find emergencies, and get in touch with medical staff. It can also help start quick, proactive treatment. This healthcare system makes it less likely that people will make mistakes or take too long to communicate, and it gives doctors more time to make decisions based on accurate observations [25]. Academic institutions and the commercial healthcare sector are devoting a significant amount of attention to the development of intelligent medical sensors, gadgets, cloud computing, and other technology related to healthcare. As a result of this, the Internet of things (IoT) has been identified as one of the most promising research subjects in the field of healthcare, namely, in the field of medical image processing. When conducting their analysis of medical photographs, researchers used a wide variety of machine learning and semisupervised learning, deep learning strategies, and artificial intelligence. These newly discovered methods are used in the process of illness detection, with the goal of assisting medical professionals in the early phases of disease diagnosis, as well as delivering findings that are accurate, consistent, efficient, and quick, and so lowering the mortality rate. In today's world, the coronavirus (COVID-19) has emerged as one of the most challenging and serious illnesses, and it is rapidly spreading around the globe [26]. The authors conducted an exhaustive study of the applications of WMSs as well as their advancements, and they compared the performance of WMSs to that of other platforms. The authors went through the benefits that these applications of these devices bring to the table when it comes to monitoring the health of people with illnesses such as cardiac arrest and Alzheimer's disease [27]. The Internet of things offers potential solutions that might reduce the load that is placed on healthcare institutions. For instance, RFID systems are used in medical institutions in order to both lower overall medical costs and improve the quality of treatment that is provided. Patients' cardiac impulses may be conveniently monitored by physicians thanks to healthcare monitoring schemes, which help physicians deliver an accurate diagnosis and improve patient care [28]. The authors [29] have shown a semisupervised learning model for the purpose of collecting the best possible collection of picture attributes. The primary focus of the ensemble learning model that has been provided is on the fact that the framework is taught to acquire various degrees of semantic representation of pictures in order to extract features of a better quality. In this way, the new set of features may be learnt with a bigger dataset via the process of constructing a more refined model. The expected fine-tuning CNN design makes use of a standard amount of medical picture attributes taken from a variety of modalities. Cloud computing (CC) is a model of distributed computing that makes it possible for companies and individual users to access virtualized computing, storage, and networking resources via the use of the Internet. At the moment, it is more economical, less difficult to manage, and more elastic to use these resources rather than a collection of local,

Table 1: Comparative analysis of recent work.

References	Study	Enhancement method	Modality	DNNs
[42]	Diabetic retinopathy	Green channel+CLAHE	Fundus images	U-Net
[43]	Retinal blood vessel segmentation	CLAHE	Fundus images	Encoder-decoder CNN
[44]	Tuberculosis detection	CLAHE, HEF, and UM	X-ray	EfficientNet-B4, ResNet-18, and ResNet-50
[45]	COVID-19	Pipeline for advanced contrast enhancement	Computed tomography (CT)	—
[46]	Medical images	UM	X-ray and CT	—
[47]	Pneumonia infection	CLAHE	X-ray	MobileNetV2 and EfficientNet: B0
[48]	COVID-19	AMF, NLMF, and CLAHE	X-ray	KL-MOB

Table 2: MURA-bone classification X-ray dataset.

Study of various parts	Training set	Testing set	Verification set
Elbow	2920	80	10
Finger	3130	79	13
Forearm	1160	62	8
Hand	4060	75	25
Humerus	670	61	9
Shoulder	4210	61	7
Wrist	5760	120	20
Total	21910	538	92

Complete dataset size: 22540.

physical ones. Cloud services are often kept in data centres, which typically consist of thousands upon thousands of individual computers [30]. In order to enhance the effectiveness of monitoring in IoT-based healthcare systems, a significant amount of research has been conducted. In this paper [31], the architecture that is employed in the Internet of things, particularly the cloud-integrated systems, is studied. In the Internet of things, accuracy and power consumption are two of the most essential concerns; as a result, this article discusses the research activities that are now underway to improve the functionality of healthcare systems that are based on the Internet of things. An expert application system has been developed [32] using the Internet of medical things (IoM). Collecting and analysing patients' physiological data are one of its primary functions to conduct a hands-on analysis of the medical sensor nodes that have been implanted into the body of the patient. In turn, it would detect the medical information of the patient utilising sophisticated portable gadgets. The security, protection, and privacy of medical data are becoming more complex issues for the Isle of Man as a result of the fact that patient information is very sensitive and should not be disclosed to anybody other than a medical expert. For this reason, a user authentication mechanism that is based on anonymity is recommended as the best solution to the problems with privacy preservation in the IoM.

The authors used transfer learning to train both DenseNet-161 and ResNet-50, deprived of using a fully linked layer to get the desired results [33]. Their study used the Kimia Path24 dataset, which was available in grayscale and colour. A grayscale dataset was utilized using the DenseNet-161 algorithm, while the ResNet-50 algorithm used a colour dataset to obtain a classification accuracy of 98.87 percent. An updated ResNet model was presented [34]. Instead of global average pooling, authors added adaptive dropout. It achieved 87.71 percent classification accuracy in Montgomery County, 62.9 percent in NIH, and 81.8 percent in Shenzhen.

The STARE dataset was used in the research by the authors [35]. The dataset has been resized into three different datasets with resolutions of 31×35 pixels, 46×53 pixels, and 61×70 pixels and has been classified into 15 dissimilar eye diseases. The investigations found that the used datasets with sizes of 32×36 and 62×72 pixels had the maximum accuracy during training. In contrast, the input test dataset with sizes of 32×36 had the highest accuracy of 80.93 percent (for the input test dataset). Mahbod et al. [36] looked at dermoscopic picture collections with dimensions ranging from 64×64 pixels to 768×768 pixels. The author concludes that the classification performance of the small-sized dataset 64×64 pixels has been significantly reduced. In contrast, the classification performance of the large-sized dataset 128×128 pixels has shown significant improvement.

The X-ray picture has improved clarity and contrast as a result of the enhancement. Using the Gaussian high-pass filter as a starting point, this filter has been optimized to have

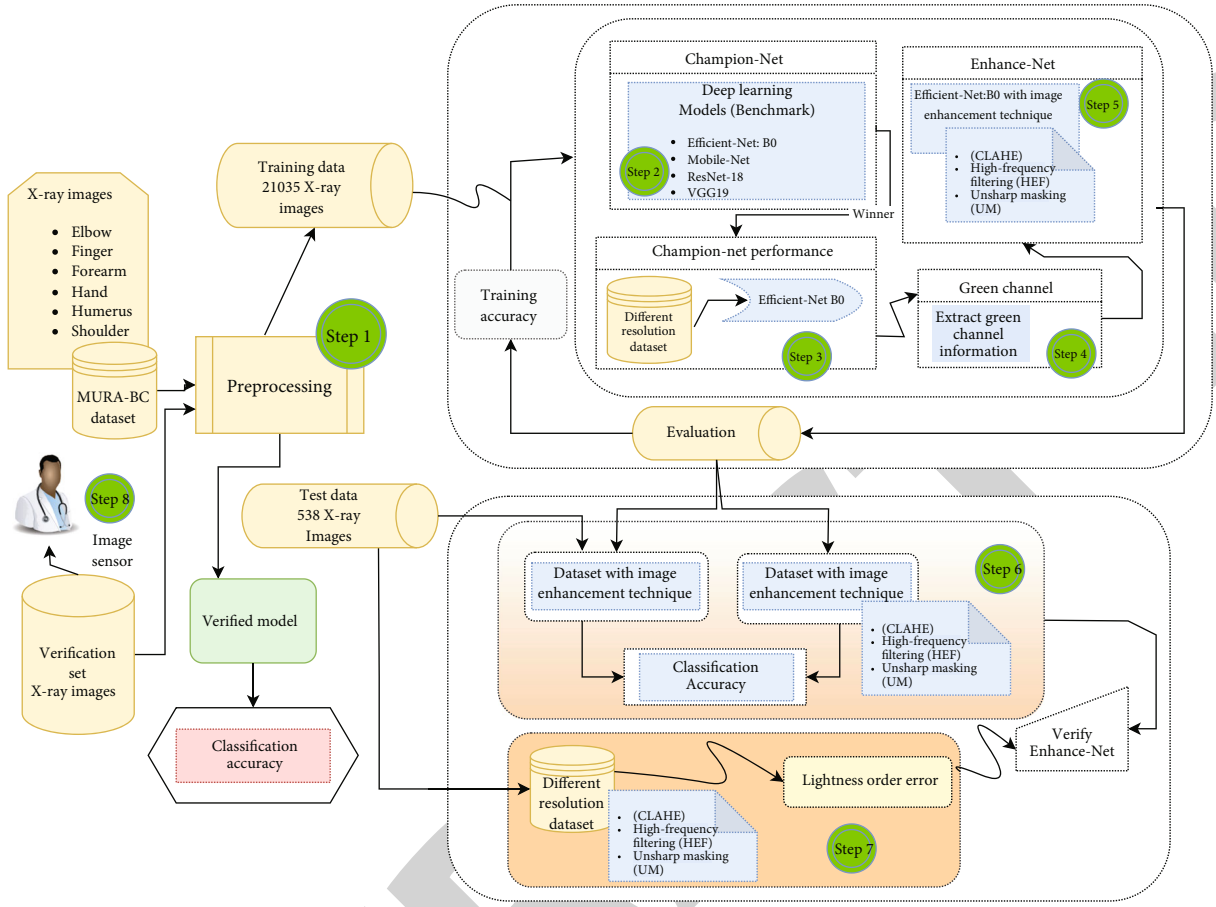

Figure 1: Block design of the proposed model.

Table 3: Parameters used for the enhancement techniques.

Enhancement model	Parameters
CLAHE	Clip limit: 40 Window size (Ws): 8 × 8
HEF	D_0: 72
UM	Amount: 2 Radius: 5

offset = 0.5 and cutoff frequency = 0.05, respectively. In [37], the authors discussed a novel nonlinear UM enhancement model (NLUM) developed to increase the fine details in mammograms, aiding in diagnosing and treating breast cancer.

A new approach for determining CLAHE algorithm hyperparameters has been developed to generate images with improved contrast [38]. It prevents the intensity values of each tile histogram from exceeding the desired clip limit by setting a clip limit. According to [39], their research aims at examining and evaluating the accuracy of various picture quality improvement strategies. Another way of putting it is that the approaches of histogram equalization (HE), gamma correction (GC), and CLAHE preprocessing are being compared. According to the findings of this study, GC has the highest sensitivity, whereas CLAHE has the highest accuracy in detecting GC. According to [40] research, the CLAHE and adaptive histogram equalization (AHE) methods are used to identify COVID-19 using the VGG19 model, with the goal of identifying COVID-19 [41] using the VGG19 model. Table 1 presents a comparative analysis of recent research findings.

3. Materials and Methods

In the musculoskeletal-based radiograph (MURA) (Rajpurkar et al., 2017), around 40500 X-ray images are gathered in one collection and used to diagnose musculoskeletal disorders. The dataset contains X-ray images that are 55.63 percent normal and 44.36 percent abnormal, respectively. The train and test datasets are organized into three sets (train, test, and verification). Every set includes seven subsets, one for each of the seven study joints: the shoulder (shoulder joint), elbow (elbow joint), humerus (humerus joint), finger (finger joint), wrist (wrist joint), and hand (hand joint). The MURA dataset was used to extract only normal X-rays, which were then used to create this dataset. Table 2 contains a detailed description of the X-ray dataset.

3.1. Various Image Enhancement Models. The representation of computation for various image enhancement approaches is discussed as follows:

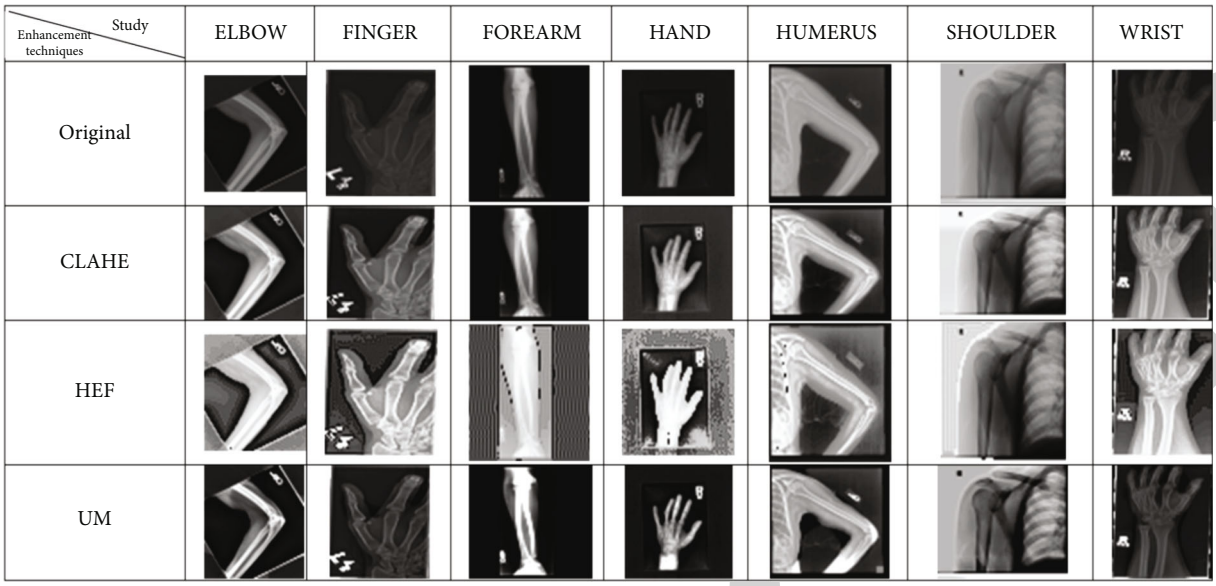

Figure 2: Outcomes of the enhancement techniques.

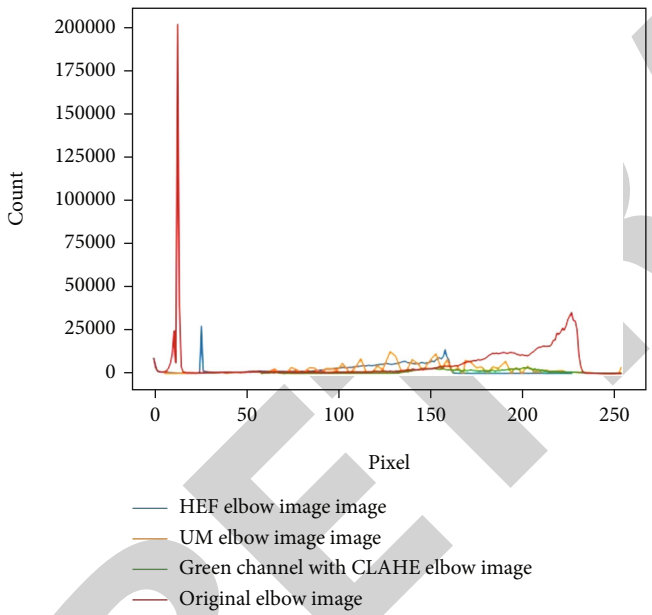

Figure 3: Histogram of MURA-BC-based random elbow image.

3.1.1. CLAHE. It is an image enhancement model [49] that has two important parameters: (1) Clip limit (C_{limit}), and (2) nonoverlapping regions ($Y_{\text{contextual}}$). The two parameters used in this model are responsible for controlling the enhanced quality of the image. X_{av} is the average amount of pixels in the grayscale computed as depicted in

$$X_{\text{av}} = \frac{X_{\text{crX}} \times X_{\text{crY}}}{X_g}, \tag{1}$$

where X_g is the gray level count in the $Y_{\text{contextual}}$, X_{crY} is the pixel count in the y dimensions $Y_{\text{contextual}}$, and X_{crX} is the pixel count in the x dimensions of $Y_{\text{contextual}}$.

Table 4: Accuracy rate of various DLMs in the training phase.

Top five training accuracy					
Epoch	EfficientNet: B0	Epoch	ResNet-18	Epoch	VGG-19
20	92.12355	19	92.05999	20	91.96678
19	92.01339	20	92.05999	19	91.96578
17	91.84815	18	92.02763	18	90.844
16	91.67443	17	92.01863	17	90.53046
18	91.65749	16	92.01763	16	90.19998
Max %	92.12355	Max %	92.05999	Max %	91.96679

$$X_{\text{acis}} = \frac{X \sum c}{X_g}. \tag{2}$$

The distributed pixel is calculated and shown in

$$\text{Pd} = \frac{X_g}{X_{\text{lp}}}, \tag{3}$$

where X_{lp} is the remaining amount of clipped image pixels.

3.1.2. HEF. HEF is an image enhancement methodology based on a Gaussian filter to improve the sharpness of the edges in an image (Bundy and Wallen. 1984). The radius of the algorithm represents the sharpness intensity of the original image, which has been transformed and filtered using the filter function and Fourier transformation. A filtered image will be produced as a result of the inverse transformation. Second, the image's contrast is in sync with the histogram equalization setting on the computer. The Gaussian-based high-pass filter is computed in the manner

Table 5: Accuracy rate of testing of various deep learning-based models.

Top five test accuracy					
Epoch	EfficientNet: B0	Epoch	ResNet-18	Epoch	VGG-19
19	91.30174	20	90.50178	20	88.1824
17	90.94181	19	90.40192	19	87.7625
16	90.16197	18	90.16197	18	89.802
9	89.0222	13	90.10198	17	88.0624
11	89.0222	12	89.86203	16	88.3623
Max %	91.30174	Max %	90.50178	Max %	89.802

Table 6: Error rate during the training phase of DLMs.

Top five training error rate							
Epoch	EfficientNet-B0	Epoch	MobileNet	Epoch	ResNet18	Epoch	VGG19
19	0.241755	19	0.269972	19	0.242157	19	0.26715
20	0.244397	20	0.275724	20	0.242157	20	0.26815
18	0.259444	18	0.295539	18	0.249675	18	0.30285
17	0.260169	17	0.306982	17	0.249775	17	0.30717
16	0.262874	16	0.333399	16	0.249875	16	0.319
Min %	0.241755	Min %	0.269972	Min %	0.242157	Min %	0.26715

Table 7: Error rate during the testing phase of DLMs.

Top five test error rate							
Epoch	EfficientNet: B0	Epoch	Mobile-net	Epoch	ResNet-18	Epoch	VGG-19
19	0.276527	12	0.291593	20	0.293466	18	0.32459
16	0.300061	16	0.296771	13	0.296771	16	0.37789
17	0.327415	19	0.298766	19	0.298766	20	0.38395
9	0.338509	10	0.303375	17	0.306369	17	0.40352
11	0.345888	15	0.317347	18	0.312	19	0.41603
Min %	0.276527	Min %	0.291593	Min %	0.293466	Min %	0.32459

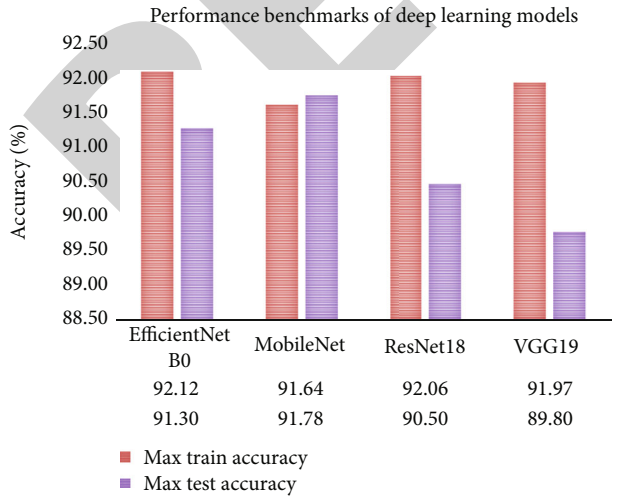

Figure 4: Training and testing accuracy of various DLMs.

shown in the diagram:

$$\text{Gau}_{\text{\_filter(x,y)}} = 1 - e^{-D^2(x,y)/2D_0{}^2}, \tag{4}$$

where D_0 is the cutoff distance. $F(i, j)$ is the Fourier transform computes as shown in

$$F(i,j) = \sum_{x=0}^{h-1}\sum_{y=0}^{w-1} f(x,y)e^{-j2\pi((\text{ix}/h)+(\text{jy}/w))}, \tag{5}$$

where i and $x = 0, 1, 2, \cdots \cdots h - 1$ and j and $y = 0, 1, 2, \cdots w - 1$. $F(x, y)$ is the inverse Fourier transformation computed as shown in

$$F(x,y) = \frac{1}{\text{hw}}\sum_{x=0}^{h-1}\sum_{y=0}^{w-1} f(i,j)e^{-j2\pi((\text{ix}/h)+(\text{jy}/w))}. \tag{6}$$

3.1.3. UM. UM is a kind of image enhancement method used to sharpen an image that has been captured (Polesel,

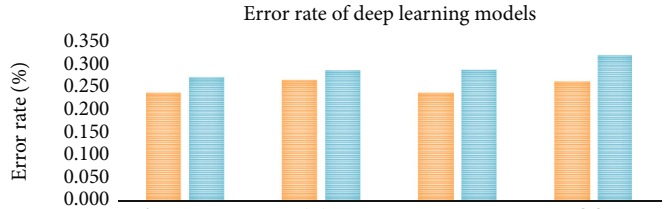

	EfficientNetB0	MobileNet	ResNet18	VGG19
Min train error rate	0.242	0.270	0.242	0.267
Min test error rate	0.277	0.292	0.293	0.325

Figure 5: Training and testing error rate of various DLMs.

Ramponi and Mathews, 2000). The sharp details of the image are computed as a difference between the original image and the image with Gaussian blur applied to the original image. The input image is blurred using a Gaussian blur filter at the beginning of this technique. The radius of the blur and the amount of blur are the two key parameters for Gaussian blurry images (Ramponi, 1998). The radius has an effect on the size of the edge that needs to be enlarged. According to equation (7), the amount of darkness, lightness, and contrast is included in the edges of the images.

$$G(x, y) = \frac{1}{2\pi\sigma^2} e^{-\left(\left(x^2+y^2\right)/\left(2\sigma^2\right)\right)}, \tag{7}$$

where x, y is the horizontal and vertical distances from the source and σ is the Gaussian distribution. I_{enhanced} is the obtained image after enhancement as shown in

$$I_{\text{enhanced}} = \left(I_{\text{original}} + \text{contrast}_{\text{value}} * \left(I_{\text{blur}}\right)\right), \tag{8}$$

where I_{original} is the original image and I_{blur} is the unsharp image.

4. Proposed Work

The proposed model is divided into four major phases: image preprocessing, a benchmark-based DLM training and validation from scratch, Champion-Net used with various resolution datasets, and the application of image enhancement models. The main features of the proposed model are the selection of the Champion-Net from the deep learning technique and the implementation of image enhancement models to improve the overall performance of the Champion-Net. The performance of Enhance-Net techniques is validated using the lightness order error (LoE). The block design of our proposed paradigm is depicted in Figure 1.

4.1. Research Environment. The virtual environment was used to conduct the research. The Ubuntu operating system has 12 GB of RAM, with six virtual CPU (Intel Xeon 2.2 GHz) processors in the server that are installed on the host virtual machine. The proposed experiment takes place in a CPU-based setting, and Python 3.0 is used for the simulation process.

4.1.1. Image Preprocessing Stage. In This stage, the preprocessing of X-ray images improves the raw image's important information. The dataset creation and transformation are two steps in the image preprocessing process.

4.1.2. Image Dataset Formation. In this stage, the MURA-BC-based X-ray data is used in different pixel computations for dataset formation such as 32×32, 40×40, 48×48, 56×56, 64×64, 72×72, 80×80, and 88×88 pixels. The dataset is arranged in two packages: train and test. In the training package, around 21935 images are placed, and the test package contains 650 X-ray image samples from seven different groups.

4.1.3. Data Transformation. This step involves randomly cropping both the training and testing datasets with the four padding and flipping X-ray images in horizontal and flipping the training dataset. This strategy gives you an advantage over the rest of the dataset. The normalizing procedure is used to minimize signals that include undesired noise or distortion. Because of uneven staining and insufficient contrast, the X-ray picture acquired by the imaging modality system may be partial and lacking in important features, such as the patient's position.

4.2. Benchmark of Deep Learning-Based Model Training and Validation. This study started with a clean slate and trained the benchmark of deep learning-based models (EfficientNet: B0; MobileNet; ResNet18; and VGG19) from the ground up. This dataset of 3232 X-ray images from the MURA-BC experiment was used for train, validation, and testing.

4.3. Champion-Net Processed with Different Resolution Dataset. The performance of a DLM trained on datasets with different resolutions (4040, 4848, 5656, 6464, 7272, 8080, and 8888 pixels) was determined in this phase using different resolution datasets. This step will assist us in determining the best deep learning model from the deep learning models available.

4.4. Green Channel Extraction. The suggested model is designed to extract the green channel details and convert the image into a grayscale. In [50, 51], the authors have used only the green channel of the RGB colour image for conversion to a grayscale image. The green channel image keeps the most information. The green channel of fundus pictures is often utilized since several authors' findings have shown that

Table 8: Champion-Net performance based on various training datasets.

Training report															
Epoch	EfficientNet: B0 32 × 32	Epoch	EfficientNet: B0 40 × 40	Epoch	EfficientNet: B0 48 × 48	Epoch	EfficientNet: B0 56 × 56	Epoch	EfficientNet: B0 64 × 64	Epoch	EfficientNet: B0 72 × 72	Epoch	EfficientNet: B0 80 × 80	Epoch	EfficientNet: B0 88 × 88
20	92.12	16	93.07	19	92.54	20	92.55	20	93.1	12	93.89	19	94.64	18	94.86
19	92.01	19	92.94	17	92.33	18	92.3	16	93.03	15	93.86	18	94.55	19	94.5
17	91.84	20	92.74	20	92.33	19	92.3	12	93	14	93.77	17	94.53	16	94.47
16	91.67	18	92.65	14	92.29	16	92.18	19	92.94	18	93.71	12	94.39	13	94.45
18	91.65	13	92.63	18	91.99	17	92.14	18	92.89	20	93.7	13	94.39	11	94.44
Max %	92.12	Max %	93.07	Max %	92.54	Max %	92.55	Max %	93.1	Max %	93.89	Max %	94.64	Max %	94.86

Table 9: Champion-Net accuracy of various resolution test datasets.

Testing report															
Epoch	EfficientNet: B0 32 × 32	Epoch	EfficientNet: B0 40 × 40	Epoch	EfficientNet: B0 48 × 48	Epoch	EfficientNet: B0 56 × 56	Epoch	EfficientNet: B0 64 × 64	Epoch	EfficientNet: B0 72 × 72	Epoch	EfficientNet: B0 80 × 80	Epoch	EfficientNet: B0 88 × 88
19	91.3	16	93.07	10	89.74	16	90.76	18	91.96	10	92.02	16	94.24	8	92.86
17	90.94	19	92.94	7	89.68	14	90.46	17	91.3	14	91.9	20	93.46	4	92.38
16	90.16	20	92.74	6	89.2	18	89.92	15	90.94	8	91.84	19	92.8	13	92.32
9	89.02	18	92.65	14	89.08	20	89.92	11	90.58	13	91.78	17	92.68	19	92.14
11	89.02	13	92.63	8	88.66	19	89.38	9	89.8	17	91.42	14	91.96	14	91.84
Max %	91.3	Max %	93.07	Max %	89.74	Max %	90.76	Max %	91.96	Max %	92.02	Max %	94.24	Max %	92.86

Table 10: Champion-Net training time for different resolution datasets.

Champion-Net with different image resolutions	Training time for 20 epochs
EfficientNet: B0 resolution 32 × 32	30 minutes
EfficientNet: B0 resolution 40 × 40	55 minutes
EfficientNet: B0 resolution 48 × 48	1 hour 50 minutes
EfficientNet: B0 resolution 56 × 56	2 hours 45 minutes
EfficientNet: B0 resolution 64 × 64	3 hours 20 minutes
EfficientNet: B0 resolution 72 × 72	5 hours
EfficientNet: B0 resolution 80 × 80	7 hours 50 minutes
EfficientNet: B0 resolution 88 × 88	Ours

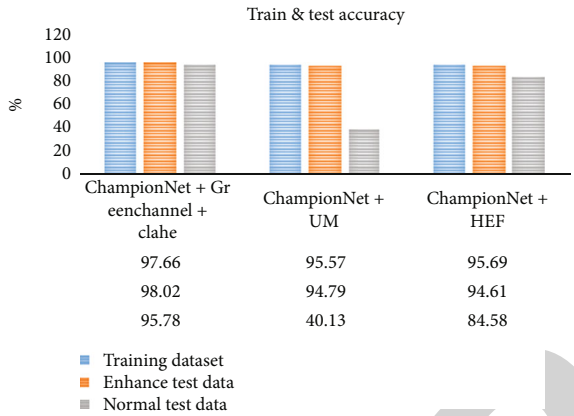

Figure 6: Dataset of training and testing accuracy (with and without enhancement).

the green channel of the RGB representation of retinal fundus images provides the most significant contrast. This is why the green channel of fundus images is so commonly used [52].

4.5. Image Enhancement Techniques. In total, three well-known enhancement techniques, (1) CLAHE, (2) HEF, and (3) UM, are developed in this paper. The parameters of enhancement techniques are listed in detail in Table 3 of this document. Figure 2 shows the results of enhancement techniques applied to a few of the input X-ray samples. In Figure 3, we showed a histogram chart representing the elbow bone images using MURA-BC data that were randomly selected.

5. Results and Its Validation

The proposed model's simulation is divided into three primary parts: (1) benchmark deep learning, (2) model training, and (3) validation. Champion-Net processing was done with various resolution datasets and application of image enhancing algorithms on Champion-Net. All three phases were simulated using Python 3.0.

The accuracy (Acc) and error rate (Er) of our model are used to assess its performance. Validation is carried out by using LoE.

5.1. Accuracy. The accuracy is the percentage of successfully categorized photos in the dataset (Mall, Singh, and Yadav, 2019) [53]. The parameter "accuracy" is computed as shown in (9) as follows:

$$A_{cc} = \frac{\text{TP} + \text{TN}}{\text{total number}}. \tag{9}$$

The total amount of the dataset for the images is computed as shown in (10) as follows:

$$\text{Total number} = (\text{TN} + \text{TP} + \text{FP} + \text{FN}), \tag{10}$$

where TN is the true negative, TP is the true positive, FP is the false positive, and FN is the false negative.

5.2. Order of Error. The naturalness of an image is critical for image enhancement approaches, yet the majority of these techniques are unable to adequately retain the naturalness of the image. Among the approaches (HEF, UM, and CLAHE) that have been examined, this IQA methodology delivers the most comprehensive answer. The difference between the original sample input picture I_{input} and the improved image I_{enhanced} is used to calculate the level of entropy. Having a low LoE score suggests that you have found the greatest approach to keep the naturalness of your photographs. The LoE is calculated in the manner shown in

$$\text{LoE} = \frac{1}{h * w} \sum_{i=1}^{h} \sum_{j=1}^{w} \text{RD}(i, j). \tag{11}$$

RD(x,$y$relative)'s order difference may be expressed as h/w (height/width). The relative order difference between the original and enhanced images is determined in

$$\text{RD}(I, J) = \sum_{i=1}^{h} \sum_{j=1}^{w} (U(L(x, y), L(i, j)) \bigoplus (U(L_{\text{enhance}}(x, y), L_{\text{enhance}}(i, j))). \tag{12}$$

For example, in (13) and (14), the unit step approach computes $L(x, y)$ lightness and $U(x, y)$ and the unit step

Table 11: Champion-Net training and testing accuracy of various enhancement techniques.

Epoch	Champion-Net +green channel +CLAHE	Epoch	Champion-Net+HEF	Epoch	Champion-Net+UM	Epoch	Champion-Net +green channel +CLAHE	Epoch	Champion-Net+HEF	Epoch	Champion-Net+UM	Epoch	Champion-Net +green channel +CLAHE	Epoch	Champion-Net+HEF	Epoch	Champion-Net+UM
	Training dataset accuracy						Accuracy testing with enhancement on the test dataset						Testing accuracy without enhancement on test datasets				
20	97.66	20	95.57	20	95.69	17	98.02	20	94.79	16	94.61	18	95.78	13	40.13	18	84.58
19	96.02	18	95.27	17	95.27	15	96.63	19	93.77	18	94.39	16	94.02	12	35.93	7	77.2
17	94.87	19	95.06	16	95.26	14	94.64	16	92.93	14	93.53	20	91.6	10	35.75	9	76.72
18	94.45	17	94.99	19	95	18	97.45	17	91.2	19	93.41	15	93.06	9	34.55	3	76.66
15	94.79	16	94.74	18	94.98	12	96.42	18	90.9	20	93.11	13	91.32	18	28.49	12	75.52
Max %	97.66	Max %	95.57	Max %	95.69	Max %	98.02	Max %	94.79	Max %	94.61	Max %	95.78	Max %	40.13	Max %	84.58

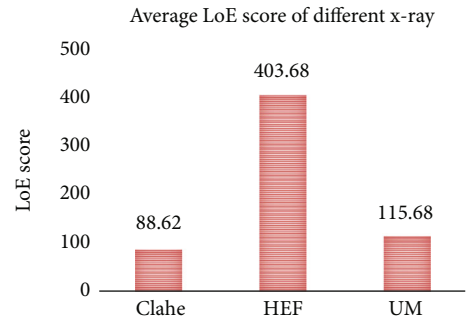

Figure 7: LoE score achieved in different image enhancement techniques.

Table 12: Different X-ray study datasets and their corresponding LoE score.

LoE_Score	CLAHE+green channel	HEF	UM
LoE_HUMERUS	85.29	585.7	104.1
LoE_SHOULDER	150.87	1.5	95.3
LoE_WRIST	53.35	403.6	83.8
Average_LoE_SCORE	88.62	402.6	115.6
LoE_ELBOW	106.87	407.9	138.8
LoE_FINGER	75.92	613.3	203.2
LoE_FOREARM	115.21	324.6	54.1
LoE_HAND	32.87	487.8	131.1

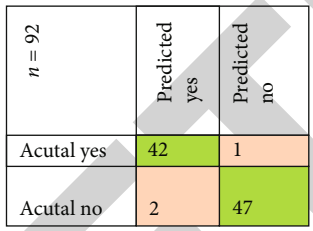

Figure 8: Confusion matrix.

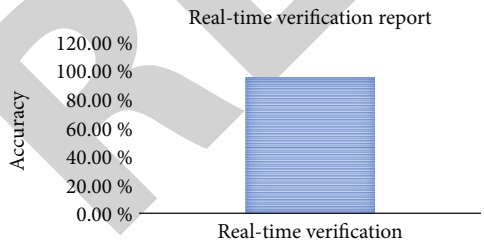

Figure 9: Real-time verification.

technique is depicted:

$$L(x,y) = \max_{c\in[r,g,b]} I^c(x,y), \tag{13}$$

$$U(x,y) = \begin{cases} 1, & x \geq y, \\ 0, & \text{else}. \end{cases} \tag{14}$$

5.3. Experiment Result for Champion-Net Selection as Winner. In order to conduct this experiment, we started with a clean slate and trained the deep benchmark learning algorithm from scratch on the MURA-BC 32 × 32 X-ray picture dataset. The model training was carried out for a total of 20 epochs. A detailed report on the training accuracy of DLMs is provided in Table 4 (EfficientNet: B0, MobileNet, ResNet-18, and VGG-19). In terms of maximum training accuracy, we achieved 92.12 percent, 91.64 percent, 92.05 percent, and 91.96 percent in the experiments.

The test accuracy of EfficientNet: B0, MobileNet, ResNet-18, and VGG-19 benchmark models is depicted in Table 5. The maximum test accuracy is calculated at 92.120%, 91.640%, 92.5%, and 91.960%.

A comparison of training error rates for the benchmark deep learning models EfficientNet: B0, MobileNet, ResNet-18, and VGG-19 is presented in Table 6. We acquire minimum training errors of 0.281, 0.4026, 0.2760, and 0.35249, for four different training scenarios.

The test accuracy of EfficientNet: B0, MobileNet, ResNet-18, and VGG-19 benchmark models is shown in Table 7. The minimum test error rate was obtained at 0.2765270, 0.2915930, 0.2934660, and 0.3245850.

As illustrated in Figures 4 and 5, the EfficientNet: B0 is selected as the Champion-Net based on the accuracy and error of training and testing. For training and testing, the highest accuracy (EfficientNet: B0) is 92.15 and 91.3, and the minimum training and testing of error rates are obtained at 0.24 and 0.27.

5.4. Experimental Result for Champion-Net Computed with Different Resolution Datasets. First and foremost, this experiment used the understanding of the link between DLM and various dataset resolutions. Second, estimate the amount of time it will take to train on various resolutions. The findings in Table 7 and Table 8 demonstrate the impact of various resolutions of X-ray image datasets on the organization using different resolution X-ray image datasets. Various resolution datasets are represented in Table 9 to help you estimate the training time. The performance of DLMs, on the other hand, improves as the resolution of the dataset increases. As the resolution of the dataset is increased, so is the amount of time spent training. As a result, it is clear from Tables 8–10 that the 64-64 pixel resolution dataset performs better in terms of accuracy and training time, while the 32-32 pixel resolution dataset performs the worst. As a result, we have chosen an image of a 64-64 pixel X-ray dataset.

5.5. Experimental Result for Champion-Net with Different Image Enhancement Techniques. The primary goal of this phase of research is to improve the overall performance of DLMs, which is now underway. We have processed the dataset that was finalized in the previous phase using several image enhancement algorithms, including HEF, CLAHE, and UM, to get the desired results. The findings in Table 10 and in Figure 6 demonstrate the organization and performance of Champion-Net along with the enhancement approaches on the datasets, in the presence and absence of

enhancement strategies, respectively. On the training dataset, the performance of all three image-enhancing algorithms is about the same in the range of 97.66 to 95.69 percent. The difference between the test datasets with and without enhancing methods was examined during the testing phase. It is evident that the green channel+CLAHE strategy surpasses both of the other two procedures, according to the results in Table 11. The green channel+CLAHE methodology obtained a 95.78 percent accuracy using enhancement techniques. HEF obtained an accuracy of 94.79 percent, while UM obtained an accuracy of 94.61 percent on the test dataset. Without the use of enhancement techniques, HEF obtained just 40.15 percent, and UM scored 84.5 percent on the test data, respectively.

5.6. Result Validation Using LoE. The low level of evidence (LoE) technique is used for result validation of the preceding phase of the experiment in the final step, as represented in Figure 7. Table 12 displays the LoE-based score of several bone X-ray scans. The lowest LoE score shows the optimal option [54], which keeps the naturalness of the photos even after they have been altered. It has a LoE of 88.62, which is the lowest of the three techniques tested. It is calculated that the HEF-based LoE score is around 403.6, whereas the UM LoE score value is around 115.6. The LoE of CLAHE verifies the outcome of the preceding phase.

6. Real-Time Verification

In this section, radiologists and orthopaedic surgeons perform real-time testing of the verified model using the trained model for real-time medical image prediction. They tested a total of 92 X-ray images. Figure 8 provides the details regarding the confusion matrix. The 96.74% accuracy is achieved during real-time testing, as shown in Figure 9. The suggested model produced the best result and improved classification performance during the experiments.

7. Conclusion

This paper has proposed a methodology for improving digital learning environments in the medical imaging field. The importance of the Internet of things in medical imaging technology is shown by how it is used in healthcare applications. We have also carried out a number of tests to enhance the overall accuracy of the proposed model and validate the findings through LoE techniques. The Champion-Net evaluation system was chosen from among the benchmark DLMs based on the accuracy and error rate of the data. Various resolutions are evaluated by the Champion-Net dataset in order to achieve the maximum possible Champion-Net performance. As part of the improvement phase, the green channel details are retrieved and retrained, and the best model is tested using image-enhancing techniques such as CLAHE, HEF, and UM.

This phase contributes to the production of Enhance-Net with improved performance. At the conclusion of the trial, we compare the findings of the Enhance-Net with the lightness order error (LoE). Using the suggested architecture of Enhance-Net, the performance of the DLMs on the MURA-BC dataset is improved significantly. The Enhance-Net makes a significant contribution to IoT-based real-time prediction models on X-ray datasets in a dynamic manner. Results of the research include X-ray pictures that have been processed with green channel+CLAHE enhancement techniques in order to increase the performance of the DLM. In the future, The Enhance-Net can also be implemented for various other medical imaging problems. This approach offers medical practitioners an instant, comprehensive tool to help them through the treatment process in a variety of medical disciplines. Despite the fact that this study is confined to X-ray image modality, the same work may be expanded to include other medical acquisition methods in the future.

Data Availability

Dataset will be made available on request.

Ethical Approval

This paper does not contain any studies with human or animal subjects.

Conflicts of Interest

The authors declare that they have no conflicts of interest.

References

[1] S. Balhara, N. Gupta, A. Alkhayyat et al., "A survey on deep reinforcement learning architectures, applications and emerging trends," *IET Communications*, vol. 16, no. 20, 2022.

[2] B. Preveze, A. Alkhayyat, F. Abedi, A. M. Jawad, and A. S. Abosinnee, "SDN-driven Internet of health things: a novel adaptive switching technique for hospital healthcare monitoring system," *Wireless Communications and Mobile Computing*, vol. 2022, Article ID 3150756, 11 pages, 2022.

[3] S. Srivastava and S. Sharma, "Analysis of cyber related issues by implementing data mining algorithm," in *2019 9th International Conference on Cloud Computing, Data Science & Engineering (Confluence)*, pp. 606–610, Noida, India, 2019.

[4] D. S. Al-Dulaimi, A. G. Mahmoud, N. M. Hassan, A. Alkhayyat, and S. A. Majeed, "Development of pneumonia disease detection model based on deep learning algorithm," *Wireless Communications and Mobile Computing*, vol. 2022, Article ID 2951168, 10 pages, 2022.

[5] V. Narayan and A. K. Daniel, "IOT based sensor monitoring system for smart complex and shopping malls," in *International Conference on Mobile Networks and Management*, pp. 344–354, Springer, 2021.

[6] V. Narayan, A. K. Daniel, and A. K. Rai, "Energy efficient two tier cluster based protocol for wireless sensor network," in *2020 international conference on electrical and electronics engineering (ICE3)*, pp. 574–579, Gorakhpur, India, 2020.

[7] N. M. Mamani, "Machine learning techniques and polygenic risk score application to prediction genetic diseases," *ADCAIJ: Advances in Distributed Computing and Artificial Intelligence Journal*, vol. 9, no. 1, pp. 5–14, 2020.

[8] V. Narayan, R. K. Mehta, M. Rai et al., "To implement a web page using thread in Java," *International Journal of Current Engineering and Technology*, vol. 7, no. 3, pp. 926–934, 2017.

[9] A. Kumar, K. Abhishek, C. Chakraborty, and N. Kryvinska, "Deep learning and Internet of things based lung ailment recognition through coughing spectrograms," *IEEE Access*, vol. 9, pp. 95938–95948, 2021.

[10] A. Krizhevsky and G. Hinton, "Learning multiple layers of features from tiny images," University of Toronto, Toronto, Ontario, 2009.

[11] A. Krizhevsky, I. Sutskever, and G. E. Hinton, "ImageNet classification with deep convolutional neural networks," *Advances in Neural Information Processing Systems*, vol. 25, pp. 1097–1105, 2012.

[12] V. Ravi, H. Narasimhan, C. Chakraborty, and T. D. Pham, "Deep learning-based meta-classifier approach for COVID-19 classification using CT scan and chest X-ray images," *Multimedia Systems*, vol. 28, no. 4, pp. 1401–1415, 2022.

[13] V. Narayan and A. K. Daniel, "A research protocol for detection and optimization of overlapping coverage in wireless sensor networks," *International Journal of Engineering and Advanced Technology*, vol. 8, Supplement 6, pp. 1–6, 2019.

[14] K. Simonyan and A. Zisserman, "Very deep convolutional networks for large-scale image recognition," 2014, https://arxiv.org/abs/1409.1556.

[15] S. Zagoruyko and N. Komodakis, "DiracNets: training very deep neural networks without skip-connections," 2017, https://arxiv.org/abs/1706.00388.

[16] V. Narayan and A. K. Daniel, "Design consideration and issues in wireless sensor network deployment," *Invertis Journal of Science & Technology*, vol. 13, no. 3, p. 101, 2020.

[17] D. Irfan, X. Tang, V. Narayan, P. K. Mall, S. Srivastava, and V. Saravanan, "Prediction of quality food sale in mart using the AI-based TOR method," *Journal of Food Quality*, vol. 2022, Article ID 6877520, 9 pages, 2022.

[18] M. Tan and Q. Le, "EfficientNet: rethinking model scaling for convolutional neural networks," in *Proceedings of the 36 th International Conference on MachineLearning*, pp. 6105–6114, Long Beach, California, 2019.

[19] M. Jaderberg, K. Simonyan, A. Zisserman, and K. Kavukcuoglu, "Spatial transformer networks," 2015, https://arxiv.org/abs/1506.02025.

[20] K. He, X. Zhang, S. Ren, and J. Sun, "Deep residual learning for image recognition," in *2016 IEEE Conference on Computer Vision and Pattern Recognition (CVPR)*, pp. 770–778, Las Vegas, NV, USA, 2016.

[21] A. G. Howard, M. Zhu, B. Chen et al., "MobileNets: efficient convolutional neural networks for mobile vision applications," 2017, https://arxiv.org/abs/1704.04861.

[22] V. Narayan and A. K. Daniel, "CHHP: coverage optimization and hole healing protocol using sleep and wake-up concept for wireless sensor network," *International Journal of Systems Assurance Engineering and Management*, vol. 13, Supplement 1, pp. 546–556, 2022.

[23] V. Narayan and A. K. Daniel, "A novel approach for cluster head selection using trust function in WSN," *Scalable Computing: Practice and Experience*, vol. 22, no. 1, pp. 1–13, 2021.

[24] A. Chandy, "A review on IoT based medical imaging technology for healthcare applications," *Journal of Innovative Image Processing*, vol. 1, no. 1, pp. 51–60, 2019.

[25] B. Prajapati, S. Parikh, and J. Patel, "An intelligent real time IoT based system (IRTBS) for monitoring ICU patient," in *International Conference on Information and Communication Technology for Intelligent Systems*, pp. 390–396, Springer, 2017.

[26] I. Ahmed, G. Jeon, and A. Chehri, "An IoT-enabled smart health care system for screening of COVID-19 with multi layers features fusion and selection," *Computing*, vol. 105, no. 4, pp. 743–760, 2023.

[27] R. Miotto, F. Wang, S. Wang, X. Jiang, and J. T. Dudley, "Deep learning for healthcare: review, opportunities and challenges," *Briefings in Bioinformatics*, vol. 19, no. 6, pp. 1236–1246, 2018.

[28] M. N. Birje and S. S. Hanji, "Internet of things based distributed healthcare systems: a review," *Journal of Data, Information and Management*, vol. 2, no. 3, pp. 149–165, 2020.

[29] A. Kumar, J. Kim, D. Lyndon, M. Fulham, and D. Feng, "An ensemble of fine-tuned convolutional neural networks for medical image classification," *IEEE Journal of Biomedical and Health Informatics*, vol. 21, no. 1, pp. 31–40, 2017.

[30] A. Darwish, A. E. Hassanien, M. Elhoseny, A. K. Sangaiah, and K. Muhammad, "The impact of the hybrid platform of Internet of things and cloud computing on healthcare systems: opportunities, challenges, and open problems," *Journal of Ambient Intelligence and Humanized Computing*, vol. 10, no. 10, pp. 4151–4166, 2019.

[31] S. Selvaraj and S. Sundaravaradhan, "Challenges and opportunities in IoT healthcare systems: a systematic review," *SN Applied Sciences*, vol. 2, no. 1, 2020.

[32] B. D. Deebak, F. Al-Turjman, M. Aloqaily, and O. Alfandi, "An authentic-based privacy preservation protocol for smart e-healthcare systems in IoT," *IEEE Access*, vol. 7, pp. 135632–135649, 2019.

[33] M. Talo, "Automated classification of histopathology images using transfer learning," *Artificial Intelligence in Medicine*, vol. 101, article 101743, 2019.

[34] Y. Zhang, X. Pan, C. Li, and T. Wu, "3D liver and tumor segmentation with CNNs based on region and distance metrics," *Applied Sciences*, vol. 10, no. 11, p. 3794, 2020.

[35] B. K. Triwijoyo, B. S. Sabarguna, W. Budiharto, and E. Abdurachman, "Deep learning approach for classification of eye diseases based on color fundus images," in *Diabetes and Fundus OCT*, pp. 25–57, Elsevier, 2020.

[36] A. Mahbod, G. Schaefer, C. Wang, R. Ecker, G. Dorffner, and I. Ellinger, "Investigating and exploiting image resolution for transfer learning-based skin lesion classification," 2020, https://arxiv.org/abs/2006.14715.

[37] K. Panetta, Y. Zhou, S. Agaian, and H. Jia, "Nonlinear unsharp masking for mammogram enhancement," *IEEE Transactions on Information Technology in Biomedicine*, vol. 15, no. 6, pp. 918–928, 2011.

[38] U. Kuran and E. C. Kuran, "Parameter selection for CLAHE using multi-objective cuckoo search algorithm for image contrast enhancement," *Intelligent Systems with Applications*, vol. 12, article 200051, 2021.

[39] H. Raj and D. K. Vishwakarma, "Detection of COVID-19 in chest X-ray image using convolutional neural network," in *2021 2nd Global Conference for Advancement in Technology (GCAT)*, pp. 1–5, Bangalore, India, 2021.

[40] B. K. Umri, E. Utami, and M. P. Kurniawan, "Comparative analysis of CLAHE and AHE on application of CNN algorithm in the detection of COVID-19 patients," in *2021 4th*

International Conference on Information and Communications Technology (ICOIACT), pp. 203–208, Yogyakarta, Indonesia, 2021.

[41] S. Dash, C. Chakraborty, S. K. Giri, and S. K. Pani, "Intelligent computing on time-series data analysis and prediction of COVID-19 pandemics," *Pattern Recognition Letters*, vol. 151, pp. 69–75, 2021.

[42] Y. Yan, J. Gong, and Y. Liu, "A novel deep learning method for red lesions detection using hybrid feature," in *2019 Chinese Control And Decision Conference (CCDC)*, pp. 2287–2292, Nanchang, China, 2019.

[43] Y. Wu, Y. Xia, Y. Song, Y. Zhang, and W. Cai, "NFN+: a novel network followed network for retinal vessel segmentation," *Neural Networks*, vol. 126, pp. 153–162, 2020.

[44] K. Munadi, K. Muchtar, N. Maulina, and B. Pradhan, "Image enhancement for tuberculosis detection using deep learning," *IEEE Access*, vol. 8, pp. 217897–217907, 2020.

[45] G. Siracusano, A. La Corte, M. Gaeta, G. Cicero, M. Chiappini, and G. Finocchio, "Pipeline for advanced contrast enhancement (PACE) of chest X-ray in evaluating COVID-19 patients by combining bidimensional empirical mode decomposition and contrast limited adaptive histogram equalization (CLAHE)," *Sustainability*, vol. 12, no. 20, p. 8573, 2020.

[46] I. Draganov and V. Gancheva, "Unsharp masking with local adaptive contrast enhancement of medical images," in *International Conference on Medical Imaging and Computer-Aided Diagnosis*, pp. 354–363, Springer, 2021.

[47] E. Avsar, "Effects of image preprocessing on the performance of convolutional neural networks for pneumonia detection," in *2021 International Conference on INnovations in Intelligent SysTems and Applications (INISTA)*, pp. 1–5, Kocaeli, Turkey, 2021.

[48] M. M. Taresh, N. Zhu, T. A. A. Ali, M. Alghaili, A. S. Hameed, and M. L. Mutar, "KL-MOB: automated COVID-19 recognition using a novel approach based on image enhancement and a modified MobileNet CNN," *PeerJ Computer Science*, vol. 7, article e694, 2021.

[49] K. Zuiderveld, "Contrast limited adaptive histogram equalization," in *Graphics Gems*, pp. 474–485, Elsevier, 1994.

[50] N. P. Singh and R. Srivastava, "Retinal blood vessels segmentation by using Gumbel probability distribution function based matched filter," *Computer Methods and Programs in Biomedicine*, vol. 129, pp. 40–50, 2016.

[51] S. K. Saroj, R. Kumar, and N. P. Singh, "Frechet PDF based matched filter approach for retinal blood vessels segmentation," *Computer Methods and Programs in Biomedicine*, vol. 194, article 105490, 2020.

[52] S. Gharabaghi, S. Daneshvar, and M. H. Sedaaghi, "Retinal image registration using geometrical features," *Journal of Digital Imaging*, vol. 26, no. 2, pp. 248–258, 2013.

[53] H. Panwar, P. K. Gupta, M. K. Siddiqui, R. Morales-Menendez, and V. Singh, "Application of deep learning for fast detection of COVID-19 in X-Rays using nCOVnet," *Chaos, Solitons & Fractals*, vol. 138, p. 109944, 2020.

[54] P. K. Mall and P. K. Singh, "BoostNet: a method to enhance the performance of deep learning model on musculoskeletal radiographs X-ray images," *International Journal of Systems Assurance Engineering and Management*, vol. 13, Supplement 1, pp. 658–672, 2022.